doi:10.1016/j.jmb.2005.08.041 J. Mol. Biol. (2005) 353, 308–321

JMB

Available online at www.sciencedirect.com

SCIENCE DIRECT®

ELSEVIER

Characterization of T Cell Receptors Engineered for High Affinity Against Toxic Shock Syndrome Toxin-1

Rebecca A. Buonpane[1], Beenu Moza[2], Eric J. Sundberg[2] and David M. Kranz[1]*

[1]*Department of Biochemistry University of Illinois, Urbana IL 61801, USA*

[2]*Boston Biomedical Research Institute, 64 Grove Street Watertown, MA 02472, USA*

**Corresponding author*

Superantigens, including bacterial enterotoxins, are a family of proteins that bind simultaneously to MHC class II molecules and the Vβ regions of T cell receptors. This cross-linking results in the activation of a large population of T cells that release massive amounts of inflammatory cytokines, ultimately causing a condition known as toxic shock syndrome. The staphylococcal superantigen toxic shock syndrome toxin-1 (TSST-1) is a causative agent of this disease, but its structure in complex with the cognate T cell receptor (human Vβ2.1) has not been determined. To understand the molecular details of the interaction and to develop high affinity antagonists to TSST-1, we used directed evolution to generate a panel of high affinity receptors for TSST-1. Yeast display libraries of random and site-directed hVβ2.1 mutants were selected for improved domain stability and for higher affinity binding to TSST-1. Stability mutations allowed the individual Vβ domains to be expressed in a bacterial expression system. Affinity mutations were generated in CDR2 and FR3 residues, yielding improvements in affinity of greater than 10,000-fold (a K_D value of 180 pmol). Alanine scanning mutagenesis of hVβ2.1 wild-type and mutated residues allowed us to generate a map of the binding site for TSST-1 and to construct a docking model for the hVβ2.1–TSST-1 complex. Our experiments suggest that the energetic importance of a single hVβ2.1 wild-type residue likely accounts for the restriction of TSST-1 specificity to only this human Vβ region. The high affinity mutants described here thus provide critical insight into the molecular basis of TSST-1 specificity and serve as potential leads toward the development of therapeutic agents for superantigen-mediated disease.

Keywords: bacterial superantigens; enterotoxins; toxic shock syndrome; protein engineering; yeast display

Introduction

Toxic shock syndrome (TSS) was characterized as a disease associated with staphylococci infection over 25 years ago.[1] Subsequently, toxic shock syndrome toxin-1 (TSST-1) from *Staphylococcus aureus* was identified as the protein responsible in most cases of the disease.[2,3] TSST-1 is a member of a family of molecules secreted by *S. aureus* and *Streptococcus pyogenes* that cause elevated systemic cytokine levels, including tumor necrosis factor-α (TNF-α) and interleukin-1 (IL-1), leading to fever, TSS, and ultimately organ failure.[4] The term superantigen (SAg) was given to this class of molecules because these toxins stimulate a large fraction of T cells bearing the same variable regions of the T cell receptor beta chain (Vβ regions).[5,6] As up to 20% of the T cell repertoire can bear the same Vβ region, SAgs are capable of stimulating thousands of times more T cells than conventional antigens. Since soluble monovalent ligands for the T cell receptor (TCR) cannot themselves stimulate T cells, SAgs act by cell-to-cell cross-linking TCRs and class II major histocompatibility complex (MHC) molecules on antigen presenting cells.

Abbreviations used: TSST-1, toxic shock syndrome toxin-1; TNF, tumor necrosis factor; SAg, superantigen; TCR, T cell receptor; MHC, major histocompatibility complex; CDR, complementarity determining region; FACS, fluorescence-activated cell sorting; SPR, surface plasmon resonance.

E-mail address of the corresponding author: d-kranz@uiuc.edu

The bacterial SAg family now numbers over 20 members, including the *S. aureus* enterotoxins TSST-1, A (SEA) to E, and G to Q and the *S. pyogenes* exotoxins A (SpeA), C, G to M, and the mitogenic exotoxins called SMEZ.[4] Sequence based phylogenetic relationships among these toxins indicated that they represent five groups, in which one group contains TSST-1 as the only known member.[4] The structures of SAgs, including TSST-1,[7,8] have been shown to be very similar. A smaller N-terminal domain contains two β-sheets and a larger C-terminal domain consists of a central α-helix and a five-stranded β-sheet. Although all bacterial SAgs share a common three-dimensional structure, they exhibit diversity in their specificities for TCR Vβ domains and class II MHC molecules, as well as in the molecular architecture of the respective MHC–SAg–TCR signaling complexes that they form.[9]

TSST-1 interacts almost exclusively with the human Vβ2.1 (hVβ2.1) region[10] and a significant fraction of patients with TSS exhibit expansions of T cells with hVβ2.1.[11] The structure of hVβ2.1 in complex with SpeC showed that hVβ2.1 uses a greater number of hypervariable regions for contact, compared to the interaction of mouse Vβ8.2 with its three different SAg ligands.[12] Thus, residues from all three complementarity determining regions (CDRs) and hypervariable loop 4 (HV4) contributed contacts with SpeC and the interface exhibited a greater buried surface area than mVβ8.2–SAg interfaces. While the structure of the hVβ2.1–TSST-1 complex has not been solved, a recent alanine mutagenesis study of TSST-1 revealed the key residues of TSST-1 that are involved in the interaction.[13]

Here, we have used yeast display techniques to engineer the hVβ2.1 region for improved TSST-1 binding, in order to generate affinity-matured proteins as tools for dissecting the hVβ2.1–TSST-1 interaction.[13–15] The highest affinity variant exhibited a K_D of 180 pM, primarily attributable to a significantly decreased off-rate. A survey of amino acid positions that varied with high frequency among different Vβ regions, and mutational analyses of a high-affinity hVβ2.1 variant, revealed sites on hVβ2.1 that are important for TSST-1 binding. These sites involved predominantly the CDR 2 and the framework (FR) 3 region. These analyses also revealed a key wild-type residue (Tyr56) that likely confers the strict Vβ domain specificity of TSST-1. The highest affinity variant Vβ domain fragments also serve as the foundation for neutralizing agents for the cellular events that lead to TSS.

Results

Engineering stabilized hVβ2.1 mutant by yeast display

Our previous studies have shown that single-chain TCRs (Vβ-linker-Vα) or Vβ domains required mutations to display the properly folded proteins, as a fusion to the agglutinin receptor Aga2, on the surface of yeast.[15–17] Subsequent studies showed that mutations that enabled surface display also yielded thermally stabilized, soluble V region domains that could be secreted from yeast[18] or refolded from *Escherichia coli* inclusion bodies (data not shown). To explore the feasibility of engineering the hVβ2.1 region by yeast display, a fusion of genes encoding Aga2, a hemagglutinin (HA) epitope tag, hVβ2.1, and a c-myc epitope tag (Figure 1(a)) was cloned into the yeast display vector. As anticipated, the wild-type hVβ2.1 region was not detected on the surface, as probed with a monoclonal antibody to this specific V region (Figure 1(b)) or with an antibody to the C-terminal c-myc tag (data not shown). To identify a mutated hVβ2.1 domain variant that could be displayed on the yeast surface and that might allow expression in *E. coli*, the hVβ2.1 insert was subjected to error-prone PCR at an error rate resulting in an average of two mutations per Vβ molecule. PCR products were cloned by homologous recombination into the yeast display plasmid resulting in a library size of approximately 15×10^6 transformants. The library was selected by fluorescence-activated cell sorting (FACS) with an anti-hVβ2 antibody through three rounds and an anti-c-myc antibody for one round. After the final round of selection, yeast cells were plated and individual clones were screened for binding to the hVβ2-specific antibody. Figure 1(b) shows an example of the improvement in surface display for one of the clones, EP-8.

Ten clones (designated EP-series) with the highest levels of surface hVβ2.1, as judged with an anti-hVβ2 antibody, were chosen for sequence analysis. Seven unique sequences, with two or three mutations each, were identified (Figure 2). Two of

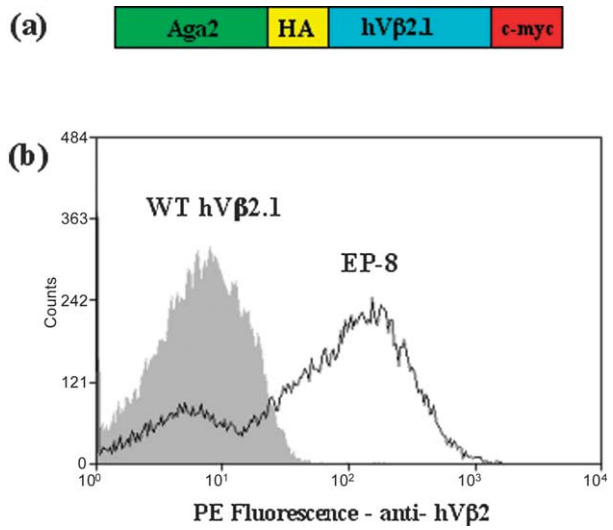

Figure 1. Yeast display of human Vβ2.1 before and after stabilization. (a) Yeast display construct of hVβ2.1. (b) Yeast cell histograms of wild-type hVβ2.1 and clone EP-8 isolated from the error-prone library after staining with an anti-human Vβ2 antibody.

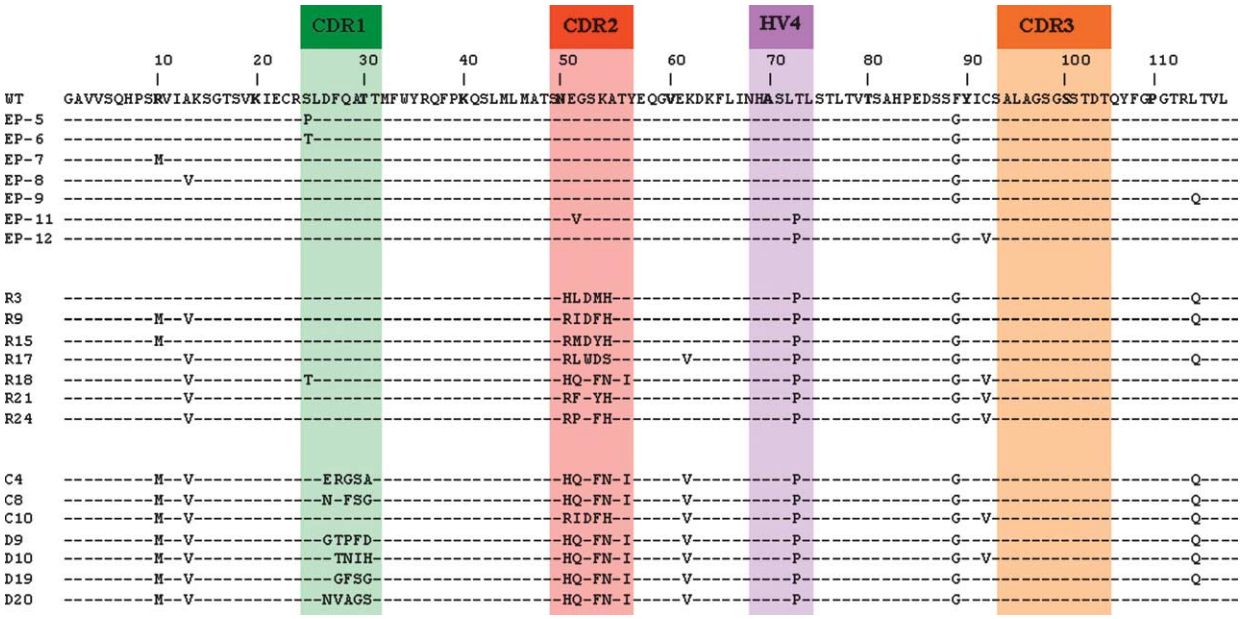

Figure 2. Sequences of hVβ2.1 mutants isolated in the yeast display system. The designation EP refers to clones isolated from the error-prone (stability) library. The designation R refers to clones isolated from the CDR2 (affinity) library. The designation C or D refer to clones isolated from the third and fourth sorts, respectively, from the combined CDR1, CDR2b, or HV4 (off-rate) library.

the mutations were present in the CDRs, one was present in HV4, and five mutations were present in FR regions. One of the FR mutations in particular, S88G, was the most prevalent of the mutations isolated, as it was found in six of the seven unique clones. Five of these mutations (R10M, A13V, L72P, S88G and R113Q) accumulated in almost every clone isolated after subsequent rounds of affinity maturation (see below), suggesting that these mutations were each important in stabilization and display. Four of the mutations are located at the Vβ surface, where the constant region (Cβ) would be located in the wild-type T cell receptor (Figure 9(a), below). In full length β chains, this area is buried at the Vβ:Cβ interface[12,19,20] and thus these mutations may act to prevent aggregation of the Vβ domain. The other mutation, L72P, is located at the other end of the Vβ region within the HV4 loop. The proline substitution may act to stabilize the local region surrounding this loop.

Isolation and characterization of first generation high affinity hVβ2.1 mutants

The low affinity of hVβ2.1 for TSST-1 (K_D= 2.3 μM)[13] prohibits the effective use of the soluble Vβ receptor as an antagonist for TSST-1-mediated toxicity. To engineer higher affinity mutants, the stabilized Vβ genes (EP-series, see above) were used as a starting point for affinity maturation. Because there is no crystal structure of the hVβ2.1–TSST-1 complex, the positions for site-directed mutagenesis were based on the structures of other Vβ-SAg complexes.[12] As CDR2 is uniformly involved in contacts with SAgs,[12,21–24] including the interaction between hVβ2.1 and SpeC,[12] this region was chosen for the first round of affinity maturation. Five residues in this loop (50, 51, 52, 52a, and 53) were mutated randomly using degenerate oligonucleotides in splice extension PCR reactions with equal amounts of six unique stabilized clones isolated from the error-prone library as templates (see Figure 2). The library of approximately 14×10^6 independent clones was sorted through four cycles using decreasing concentrations of TSST-1. The first and second sorts were performed at a TSST-1 concentration of 1.8 μM (approximately equivalent to the K_D value of the wild-type hVβ2.1–TSST-1 interaction), the third sort was performed at 900 nM TSST-1, and the fourth sort was performed at 90 nM TSST-1 (approximately 20-fold below the K_D value).

Twenty-four clones (designated R-series) were analyzed by flow cytometry for their ability to bind to 200 nM TSST-1, approximately tenfold below the K_D value of the wild-type. At this TSST-1 concentration, the stabilized clone EP-8 is weakly positive (a slight shift of the flow histogram) and the affinity-matured clone R9 was strongly positive (Figure 3(a)). Using the mean fluorescence units of each histogram, each of the 24 clones was compared to the stabilized clone EP-8 and all clones demonstrated an improvement over the stabilized mutant (Figure 3(b)), which has an affinity similar to the wild-type hVβ2.1, as measured by surface plasmon resonance (SPR) analysis (see below and Table 1).

Fifteen clones isolated from the first affinity maturation library were sequenced to examine the mutations in the CDR2 loop (Figure 2, and data not shown). Each of the clones sequenced was unique and contained a sequence that differed from the

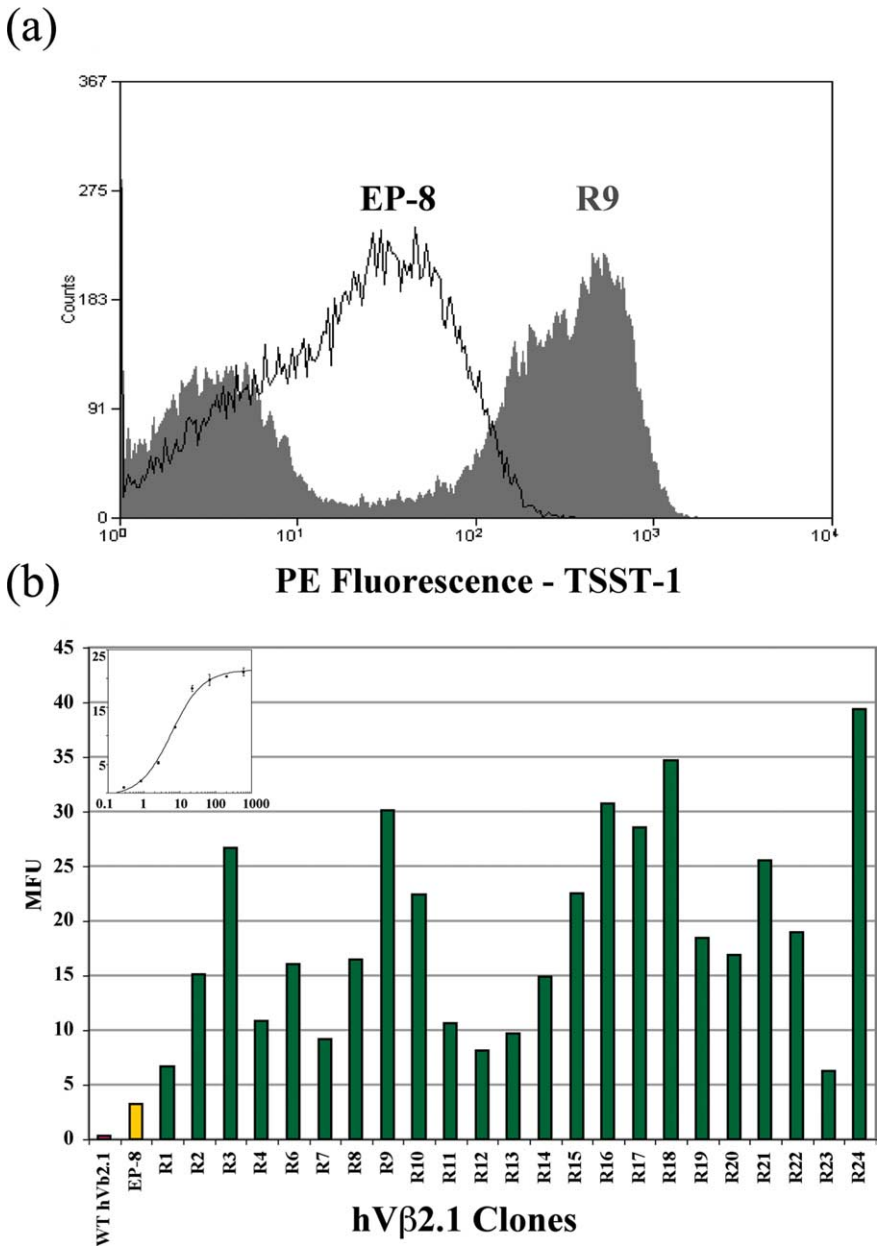

Figure 3. Binding of TSST-1 to affinity matured hVβ2.1 mutants. (a) Overlay histogram of the stabilized human Vβ2.1 clone, EP-8 (black outline), and a clone from the first-generation affinity library, R9 (gray). Yeast cells were incubated with 200 nM biotinylated TSST-1, and analyzed by flow cytometry. (b) A panel of clones isolated from the first-generation library were incubated with 200 nM biotinylated TSST-1 and analyzed by flow cytometry to determine their relative fluorescence (mean fluorescence units, MFU). Inset: a representative equilibrium binding titration of biotinylated-TSST-1 to clone R9. The *x*-axis represents the TSST-1-biotin concentration in nanomolar, and the *y*-axis represents the MFU of the samples.

Table 1. Kinetic and affinity parameters for the interactions between hVβ2.1 variants and TSST-1

	k_a ($M^{-1}\,s^{-1}$)	k_d (s^{-1})	K_A (M^{-1})	K_D (M)
EP-8[a]	n.d.[b]	n.d.	1.67×10^{6}	5.99×10^{-7}
R9	$1.48\ (\pm0.01)\times10^{4}$	$1.86\ (\pm0.02)\times10^{-3}$	7.95×10^{7}	1.26×10^{-8}
C10 (Y56A)	$5.87\ (\pm0.05)\times10^{4}$	$3.99\ (\pm0.02)\times10^{-3}$	1.47×10^{7}	6.78×10^{-8}
C10 (K62A)	$2.14\ (\pm0.01)\times10^{5}$	$3.24\ (\pm0.14)\times10^{-4}$	6.60×10^{8}	1.52×10^{-9}
C10	$3.28\ (\pm0.01)\times10^{5}$	$1.12\ (\pm0.09)\times10^{-4}$	2.94×10^{9}	3.41×10^{-10}
D10	$2.56\ (\pm0.01)\times10^{5}$	$4.59\ (\pm0.06)\times10^{-5}$	5.58×10^{9}	1.79×10^{-10}

Measured by surface plasmon resonance, with TSST-1 immobilized on chips.
[a] Affinity parameters determined by equilibrium binding studies.
[b] n.d., not determined.

wild-type CDR2 of hVβ2.1. While there did not appear to be a strict consensus of any of the residues, there were strong preferences for either histidine or arginine at position 50 (from asparagine) and a histidine at position 53 (from lysine). There were also preferences for either aspartic acid or the wild-type glycine at position 52 and an aromatic residue at position 52a. Retention of the wild-type glycine at position 52 in many clones suggests that this residue may contribute the flexibility required for positioning other residues in this loop. While CDR2 of the wild-type hVβ2.1 contains two potentially charged residues (Glu51 and Lys53) and a net neutral charge, most of the mutated CDR2 regions were highly charged with a net positive charge. The exception was clone R17 that retained a net neutral charge (see below). The preference for an aromatic residue at position 52a may also indicate a hydrophobic interaction facilitates binding to TSST-1.

Isolation and characterization of second-generation high affinity hVβ2.1 mutants

Titration of the yeast-displayed mutant R9 with various concentrations of TSST-1 yielded an estimated binding affinity of 6 nM (Figure 3(b), inset). In an effort to generate hVβ2.1 mutants with sub-

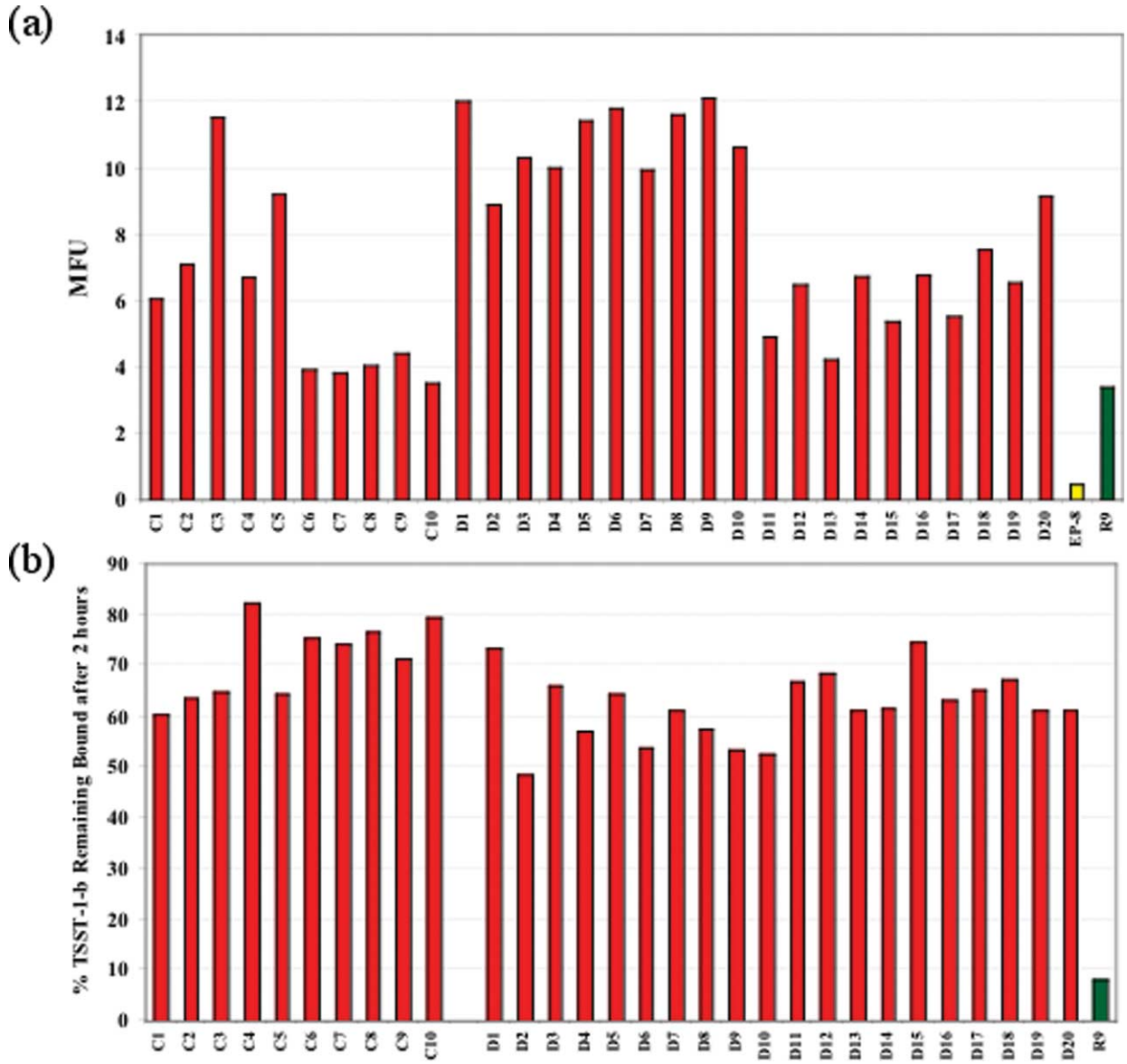

Figure 4. Binding of TSST-1 to affinity matured, second generation hVβ2.1 mutants. Analysis of the second-generation clones selected from the combined CDR1/CDR2b/HV4 libraries. (a) Equilibrium binding of clones isolated from the third (C1–10) and fourth (D1–20) rounds of sorting. Clones were incubated with 5 nM biotinylated TSST-1 followed by SA/PE and analyzed by flow cytometry. (b) Clones were incubated with 5 nM biotinylated TSST-1 for 1 h under equilibrium conditions, and then incubated with a tenfold molar excess of unlabeled TSST-1 for 2 h at 25 °C. A sample was removed before the unlabeled TSST was added and placed on ice until the end of the experiment. Percent remaining bound was calculated as (MFU after 2 h at 25 °C/ MFU at time zero) ×100.

nanomolar affinity, we used three of the first generation mutants (R9, R17 and R18) as templates for the generation of additional mutated libraries. These clones were selected on the basis of their high affinity binding to TSST-1, as well as having distinctly different CDR2 sequences (Figure 2). As hVβ2.1 binding to SpeC involves contacts with HV4 and CDR1, we reasoned that hVβ2.1 might also use these regions for binding to TSST-1. Thus, we generated separate libraries in CDR1 (residues 27, 27a, 28, 29, 30), HV4 (residues 68, 69, 70, 71, 72), and an additional library in the CDR2 loop (residues 52a, 53, 54, 55, 56) to extend the range of residues that were mutated. These three libraries were pooled in equal ratios for flow cytometric sorting.

Because the initial flow cytometry experiment determined the K_D value of hVβ2.1 mutant R9 to be about 6 nM, a selection strategy other than an equilibrium-based methodology is required. This is based on the principle that at this concentration, the number of surface displayed receptors, in a library of 10^6 yeast, begins to exceed the number of ligand molecules (in a 1 to 2 ml sample).[25] Thus, an off-rate based screening strategy[26] was adopted in an effort to isolate mutants with improved affinity exceeding that of the first-generation clones (R-series). The off-rate method involves incubation of yeast cells with labeled TSST-1 under equilibrium conditions, followed by washing and incubation with a tenfold molar excess of unlabeled TSST-1. Pilot analysis of clone R9 showed that less than 10% of biotin-TSST-1 remained bound after two hours under these conditions (Figure 4(b), and data not shown). Thus, yeast libraries were sorted after the two-hour dissociation period, and clones were isolated after the third (designated C-series) and fourth (designated D-series) cycles of selection. A total of 30 clones were examined for their ability to bind 5 nM TSST-1 in comparison to clones EP-8, R9, R17, and R18 (Figure 4(a)). Each clone exhibited binding that was equal to or better than the R-series of clones at this TSST-1 concentration. When the clones were examined using a single time-point off-rate analysis, similar to that used for sorting the library, it was evident that every clone showed significant improvements when compared to the first generation R-series clones (Figures 4(b) and 6(b), below). For example, clones R9, R17, and R18 had less than 10% of the labeled TSST-1 remaining bound after 2 h at 25 °C, while the off-rate selected clones had 50% or more of the labeled TSST-1 remaining bound.

To further examine TSST-1 off-rates, various mutants were examined for binding to labeled TSST-1 over a 5 h time period and at a higher temperature (37 °C). Histograms of clone C10 at several time points are shown in Figure 5(a). Mean fluorescence units (MFU) from histograms at various time points were plotted for each of the analyzed clones (Figure 5(b)). While bound biotinylated TSST-1 from the two first-generation clones (R9, R18) was reduced to background levels by the first time point (30 min), three clones (C4, C10 and D10) retained significant levels of bound biotinylated TSST-1 even at the end of the time

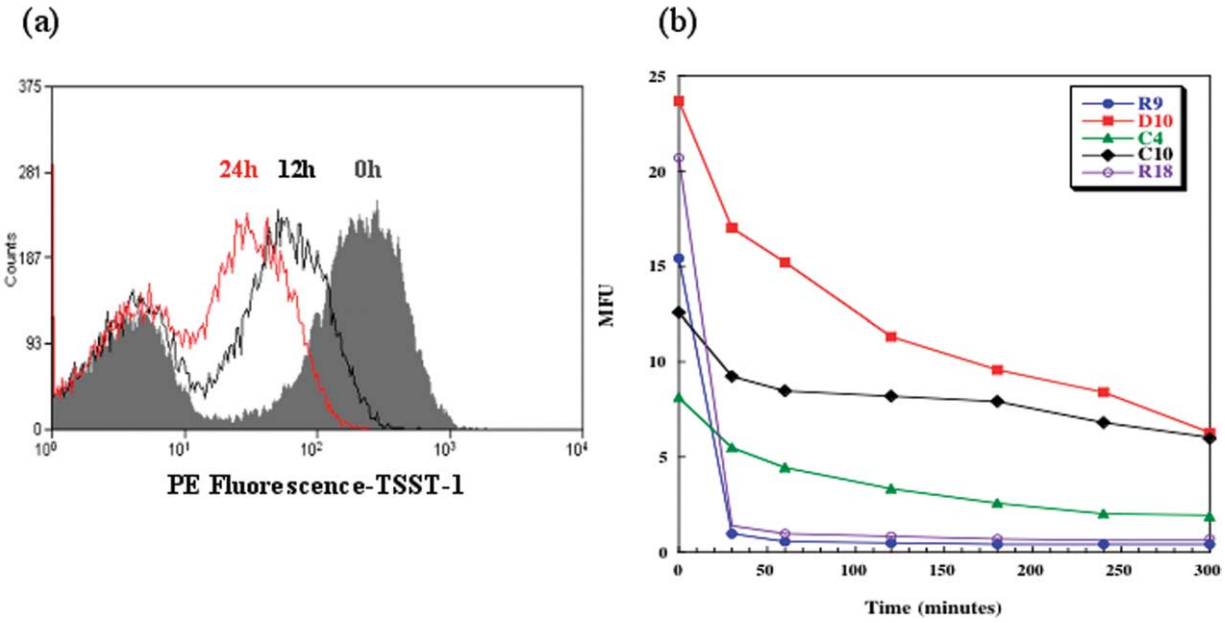

Figure 5. Off-rate analysis of TSST-1 binding to selected hVβ2.1 clones. (a) Overlay histogram demonstrating the percent biotinylated TSST-1 remaining bound to clone C10. The off-rate of clone C10 was examined by incubating the clones with 5 nM biotinylated TSST-1 for 1 h on ice, followed by incubation with a 50-fold molar excess of unlabeled TSST-1 at 37 °C. Time points were taken after 0 h (shaded gray), 12 h (black outline), and 24 h (red outline) at 37 °C. (b) Off-rate time points of first generation clones (R9 and R18) and second generation clones (C4, C10 and D10) were examined using the same experimental design as in (a).

course (5 h). Clone C10 retained approximately 50% of the TSST-1 after 5 h at 37 °C. This time course was taken out to 24 h at 37 °C, and while the levels of bound TSST-1 decreased, about 15% of TSST-1 remained bound to C10 after 24 h (Figure 5(a)).

Fourteen clones isolated from the off-rate based selection were sequenced (Figure 2, and data not shown). Eleven clones contained CDR1 mutations derived from the CDR1 library. Three clones did not contain mutations in the regions of the second-generation libraries (CDR1, CDR2 extended, and HV4), but they contained single-site mutations (e.g. clone C10). None of the clones were derived from the second extended CDR2 library, perhaps suggesting that residues 54 to 56 were critical for TSST-1 binding and their sequences could not be optimized. Each clone contained the FR3 mutation E61V, which was presumably incorporated from clone R17 through a PCR-derived error. As described earlier, each of the affinity-matured clones also contained the stabilizing mutations that may act additively in the enhanced surface display of the hVβ2.1 region, as we have observed for mutations in the 2C TCR.[16]

The absence of preferred mutations in the CDR1 clones, and the fact that clone C10 lacked CDR1 mutations altogether, suggests that CDR1 may not be involved in a significant way in binding TSST-1. Detailed inspection of the sequences indicates that the longer off-rates of these clones appear to be due to residues in the CDR2 and/or the E61V mutation, or a combination of these mutations. These possibilities are supported by mutagenesis results described below.

Alanine scanning mutagenesis of a high-affinity hVβ2.1 mutant C10

To further examine the role that the individual Vβ residues play in the interactions with TSST-1, alanine mutagenesis of selected wild-type and mutated residues of hVβ2.1 mutant C10 was performed. C10 was chosen as it exhibited high affinity with a decreased off-rate and yet contained the fewest number of mutations. Residues were chosen in part based on contact residues within the hVβ2.1–SpeC complex and also to define the mechanism by which C10 achieves high affinity.

C10 alanine mutants were constructed in the yeast display vector in order to allow rapid analysis of binding without the need for protein purification. Similar approaches have been used to examine the role of individual residues[27] or to map the binding epitopes of monoclonal antibodies.[28] Mutants were first tested for their levels of surface expression with the anti-c-myc antibody to determine if mutation to alanine affected the folding and stability of the protein. All mutants expressed detectable c-myc epitopes, with levels that were similar to or slightly improved relative to C10 Vβ (data not shown). To quantify the binding to TSST-1, each mutant was analyzed for binding to 5 and 20 nM TSST-1 and a ratio of anti-c-myc to TSST-1 binding was determined (Figure 6(a)). These concentrations of TSST-1 are about 12 and 50-fold above the estimated K_D of C10, respectively (see below), and thus were used to detect significant changes in affinity. Under these conditions, only Y56A, a mutation of a wild-type residue, was shown to affect significantly the binding of TSST-1. Further binding analysis by flow cytometry at higher TSST-1 concentrations and by SPR with soluble Y56A protein showed that TSST-1 binding affinity was reduced by ~100-fold (see below).

In order to characterize more precisely the impact of each mutation, we performed a single point off-rate analysis of the yeast-displayed mutants. Mutants were incubated with 5 nM biotinylated TSST-1, followed by incubation with a 50-fold molar excess of unlabeled TSST-1 for 2 h at 37 °C (Figure 6(b)). Time points were taken at time zero (before unlabeled ligand was added) and at 2 h to calculate the percent of remaining bound ligand. Based on this study, four alanine mutations were shown to affect the off-rate significantly: F52aA, H53A, V61A, and K62A. Mutation of these residues to alanine reduced the fraction of bound ligand to levels comparable to that of clone R9. Because two of the four residues are present in R9 (F52a and H53), we predict that residues 61 (valine) and 62 (lysine) contribute to the longer off-rate of clone C10.

It is worth noting that one clone, R17, from the first-generation of high-affinity mutants contained the E61V mutation, yet did not exhibit the slow off-rate characteristic of C10 (Figure 6(b)). The only notable sequence difference between R17 and other R-series mutants is that the net charge of the CDR2 was neutral, rather than positive. Since the H53A mutation, like the E61V mutation, appears to affect the off-rate of C10, we propose that two regions of electrostatic interactions are necessary to achieve the slow off-rate and high-affinity of C10. These regions include CDR2 and FR3.

Binding analyses of selected mutants by surface plasmon resonance

Several of the clones from the affinity maturation process, and single-site mutants, were expressed in *E. coli*, refolded from inclusion bodies, and examined using surface plasmon resonance (SPR) to measure the affinity and kinetics of their interactions with TSST-1 (Figure 7 and Table 1). As the wild-type hVβ2.1 domain does not express well in *E. coli* (data not shown), the stabilizing mutations appear to enable expression and refolding. The stabilized mutant EP-8 exhibited an affinity of 0.6 μM, similar to that observed previously for the full length wild-type hVβ2.1 (VβCβ) (K_D = 2.3 μM).[13] Based on SPR results with the higher affinity mutants, we were able to confirm findings from the flow cytometric analysis on yeast. The affinity of the first generation mutant R9 was increased by 180-fold (K_D = 12.6 nM), compared to the affinity of wild-type hVβ2.1. The affinity of the

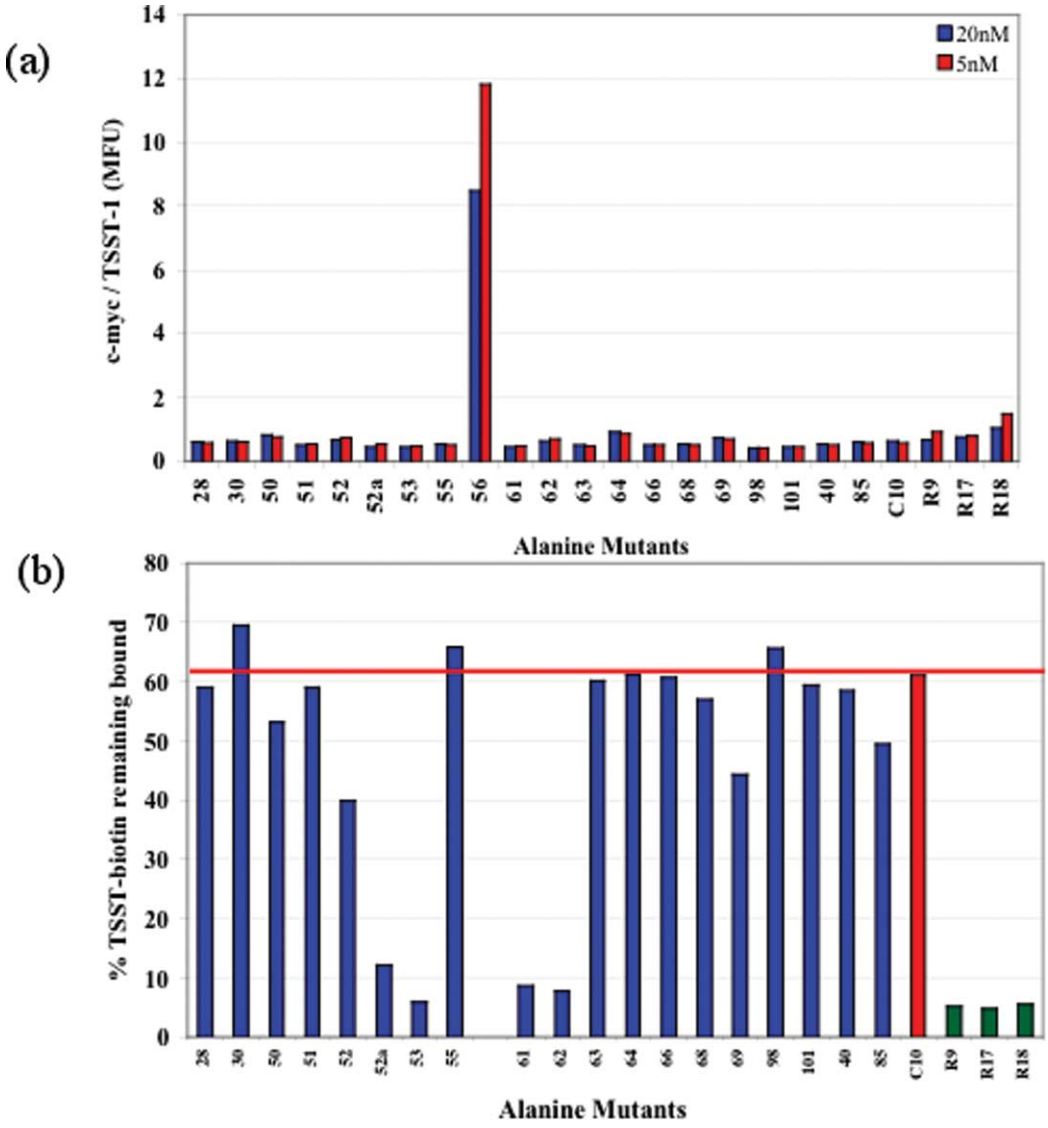

Figure 6. Binding of TSST-1 to single-site alanine mutants of hVβ2.1 clone C10. (a) Equilibrium binding of alanine mutants to c-myc antibody (which is a measure for the amount of folded protein on the cell surface; data not shown) and 5 or 20 nM biotinylated TSST-1 were used to determine the mean fluorescence units of binding. These values for c-myc and TSST-1 were used to calculate the ratio. (b) Examination of the percent biotinylated TSST-1 remaining bound after 2 h. Cells were incubated with 5 nM biotinylated TSST-1 for 1 h on ice, followed by a 50-fold molar excess of unlabeled TSST-1 for 2 h at 37 °C. A sample of the yeast was removed before transferring to elevated temperature. The red line indicates the percent of TSST-1 remaining bound to clone C10. First generation clones R9, R17, and R18 are included for comparison.

second generation mutants C10 and D10 were increased by 6800 and 12,800-fold (K_D=340 pM and 180 pM, respectively). The 180-fold higher affinity of R9 was accomplished through substitutions of CDR2 residues (residues 50–53: wild-type, NEGSK; R9, RIDFH). As indicated above, the highly charged nature of each of the CDR2 mutants may suggest that electrostatics play a role in this affinity increase. Alternatively, enhanced affinity could be achieved through an increase in the buried hydrophobic surface area. Analyses of the binding kinetics indicate that the affinity increases from R9 to C10 and D10 are due to significantly reduced off-rates (17 and 41-fold) and only modest enhancements of on-rates (2.2 and 1.7-fold). The 17-fold slower off-rate of C10 compared to R9 is consistent with the results derived from flow cytometry experiments with C10.

C10 differs from R9 at only two residues, E61V and I91V. The faster off-rate observed in the V61A mutant, and the observation that all of the second-generation clones contain the E61V mutation, suggest that this mutation accounts for the slower off-rate and corresponding increase in affinity. We speculate that this effect could be due to the loss of an acidic side-chain at position 61, enabling a productive electrostatic interaction between TSST-1 and the lysine at position 62 in hVβ2.1. In support of this possibility, the K62A mutation also resulted in a significant reduction in the

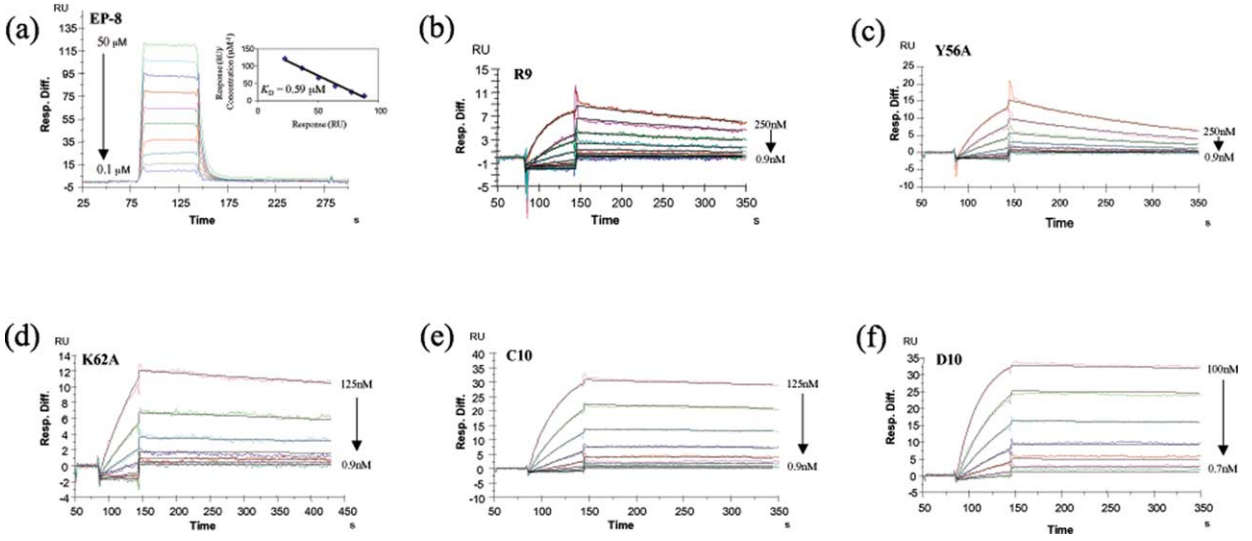

Figure 7. SPR analysis of the interactions between hVβ2.1 variants and immobilized TSST-1. The inset in (a) depicts the Scatchard analysis of equilibrium binding between EP-8 with TSST-1. Global fitting of data ((b)–(f)) to a 1:1 binding model is shown in black.

off-rate. In addition, soluble C10-K62A exhibited an affinity only twice that of R9, 17-fold reduced compared to C10 (Table 1). The lower affinity was due to a sevenfold faster off-rate and a 2.6-fold slower on-rate. Because the lysine side-chain is known to contribute to the overall hydrophobicity, we could not exclude the possibility that the K62A mutation acts through a reduction in buried hydrophobic surface area. Whatever the mechanism is, these results support the involvement of the FR3 region at positions 61 and 62 in formation and stability of the C10-TSST-1 complex.

Because Tyr56 of hVβ2.1 appeared to be the most important of the residues tested for binding to TSST-1, we examined the binding properties of the soluble C10-Y56A mutant (Table 1). The binding affinity of C10-Y56A was reduced 200-fold (K_D = 147 nM), with a 35-fold faster off-rate and a sixfold slower on-rate. While our results are based on the affinity of the engineered hVβ2.1 variant C10, the fact that Y56 is in the wild-type protein and that this residue represents one of the few unique residues of hVβ2.1 compared to other human Vβ regions,[29] suggest that it contributes significantly to the binding energy and specificity of hVβ2.1 for TSST-1.

TSST-1 and SpeC bind to overlapping epitopes on hVβ2.1

Our mutational analysis of hVβ2.1 binding to TSST-1 suggested that there might be differences compared to the binding of hVβ2.1 to SpeC (see Discussion). To determine whether there is overlap in the binding sites for TSST-1 and SpeC on hVβ2.1, a competition experiment was performed. In this experiment, SpeC was immobilized on the SPR chip, the engineered hVβ2.1 called EP-8 was injected at various concentrations, and an affinity of approximately 6 μM was measured (Figure 8(a)). To determine if TSST-1 competed for binding of the hVβ2.1 (EP-8), various concentrations of TSST-1 were mixed with 12.5 μM EP-8 (blue curve, Figure 8(a) and (b)). The ability of EP-8 to bind the SpeC was reduced as more TSST-1 was present in

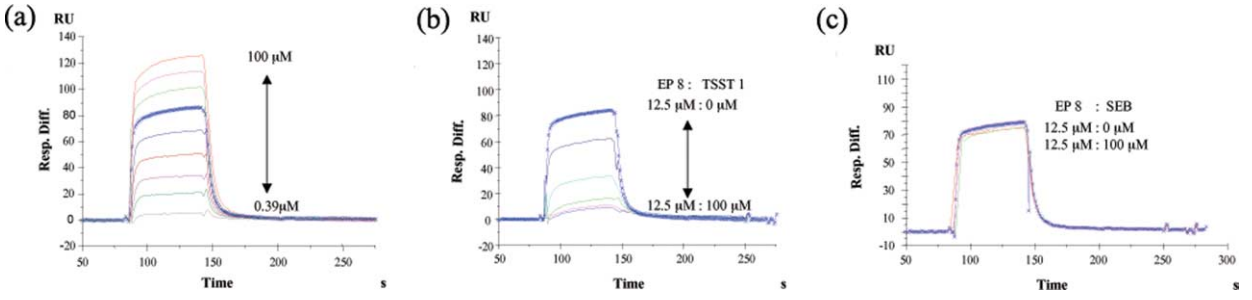

Figure 8. Competition between TSST-1 and SpeC for binding to hVβ2.1. (a) SpeC was immobilized on biosensorchip, and the stabilized hVβ2.1 mutant EP-8 was injected at various concentrations (0.39 to 100 μM) over the chip. (b) EP-8 at 12.5 μM was incubated with various concentrations of TSST-1 (0 to 100 μM) and the mixtures were injected over the chip with immobilized SpeC. (c) EP-8 at 12.5 μM was incubated with various concentrations of the SAg SEB (0 to 100 μM) and the mixtures were injected over the chip with immobilized SpeC.

the mixture (Figure 8(b)), as would be expected if there were competition for the same binding site. In a control experiment, the SAg SEB, which does not bind to hVβ2.1, was used at the same concentrations as TSST-1 and competition was not observed (Figure 8(c)).

Discussion

Secreted bacterial toxins such as TSST-1 act as SAgs by stimulating cytokine release from a large fraction of T lymphocytes.[6] The elevated systemic cytokine levels can lead to toxic shock syndrome and ultimately multi-organ failure. The mechanism of action of bacterial SAgs is now well known and a number of SAgs have been examined for the molecular basis by which they interact with T cells.[24] However, the molecular details of the interaction of TSST-1 with hVβ2.1 has so far been refractory to structural analyses. TSST-1 is particularly important clinically, as it represents one of the most common toxins involved in TSS and as such it has significant involvement in staphylococcal-mediated diseases.[4] We present here an analysis of hVβ2.1, the specific major target associated with the effects of TSST-1 in humans. The approach was to: (1) engineer a stabilized hVβ2.1 domain that would be amenable to expression in *E. coli* and directed evolution by yeast display; (2) identify specific targeted mutations in hVβ2.1 that would increase the affinity of the hVβ2.1–TSST-1 interaction; and (3) generate and analyze selected single-site mutations of hVβ2.1 that would reveal both the mechanisms by which higher affinity was achieved and the possible docking orientation of the hVβ2.1–TSST-1 complex.

The engineering of a stabilized, surface displayed hVβ2.1 mutant enabled expression of the protein in *E. coli* and subsequent refolding to concentrations sufficient for biochemical analyses. The mutations reside largely at the Vβ face, which would normally be buried at the interface with the Cβ region (Figure 9(a)). The stabilized hVβ2.1 mutant EP-8 bound to TSST-1 and SpeC with affinities that are close to those measured for the full-length β-chain. Our results also implicate the region spanning the CDR2 loop and FR3 of hVβ2.1 (including residues 51–54, 56 and 61–62) as energetically critical for TSST-1 binding. Using the hVβ2.1 as a starting point, an energy minimized model of the high-affinity mutant C10 was generated (the C10 mutations are solvent exposed). We also generated a hypothetical model of the hVβ2.1–TSST-1 complex (Figure 9(b)), by manually docking the TSST-1 in a position on hVβ2.1-C10 that is consistent with each of the following observations (described in more detail below): (1) The most important energetic residue (Tyrβ56) lies near the center of the complex; (2) the framework region 61 to 63, which was shown to be important in the engineered hVβ2.1 mutants, is in contact with a region of TSST-1 that shows electrostatic complementarity; (3) the CDR3 of hVβ2.1 which was not involved in binding based on mutational analyses, is not in contact with TSST-1; (4) TSST-1 residues that were previously identified to be important in hVβ2.1 binding are located within contact distance in the hypothetical model; and (5) the position of TSST-1 on the hVβ2.1 region overlaps that of the binding site for SpeC (Figure 9(c)) and thus SpeC binding would be competed by TSST-1.

In this model, both the positive charges on CDR2 (Arg50 and His53) and FR3 (Lys62) are positioned near negatively charged residues (e.g. Asp11 and Asp18) in TSST-1. Alternatively, it is possible that mutations such as S52aF and E61V act by increasing the buried hydrophobic surface area at the hVβ2.1–TSST-1 interface. Consistent with this possibility, the F52aA and V61A mutations both reduced the

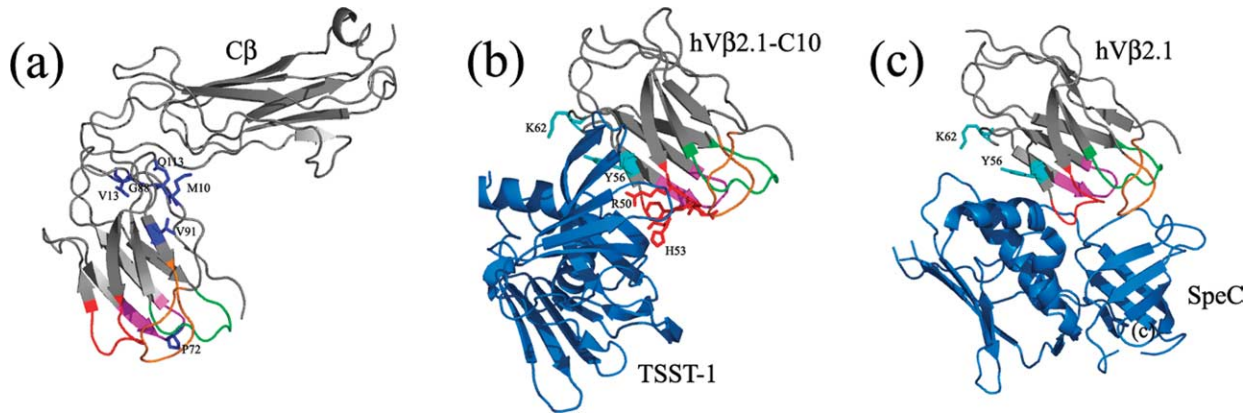

Figure 9. Model of the hVβ2.1–C10 and TSST-1 interaction. (a) Model of mutant hVβ2.1–C10 based on the structure of the wild-type human Vβ2.1. The C^{β} is included in the model for orientation. CDR1, green; CDR2, red; HV4, pink; CDR3, orange. Mutations that were isolated during the screening for yeast displayed hVβ2.1 are shown in blue. (b) Hypothetical model of the hVβ2.1–C10–TSST-1 complex. Mutated residues that were isolated during screening for higher affinity are shown in red (CDR2) or cyan (K62 and Y56). TSST-1 is shown in blue. (c) The crystal structure of human Vβ2.1 in complex with the superantigen SpeC (PDB accession code 1KTK). The Vβ domain is shown in the same orientation as in the hVβ2.1–C10–TSST-1 model for comparison. SpeC is shown in blue.

affinity, perhaps as a consequence of the reduced hydrophobicity of an alanine side-chain compared to phenylalanine and valine side-chains.

Tyrosine 56 is predicted to be at the center of the interface, in a key position to interact with TSST-1. This location is consistent with the significant energetic contribution of Tyr56 (i.e. 100-fold decrease in binding for the Y56A mutant). Our recent studies with high-affinity mouse Vβ8 mutants also showed that energetically important residues were located at the center of the interface.[30] Thus, it is reasonable to predict that Tyr56 is located at the center of the engineered hVβ2.1–TSST-1 interaction. The identification of Tyr56 as an important residue within hVβ2.1 is also consistent with the observation that this residue is nearly unique among over 50 known human Vβ regions.[29] In fact, only human Vβ4 contains a tyrosine at this position, but Vβ4 lacks positive charges in the CDR2 or at position 62 in FR3. This may explain why TSST-1 appears to be unusual among SAgs in that it is known to stimulate only a single human Vβ region, hVβ2.1.[10,11] In further support of the role of Tyr56, mouse T cells that bear mouse Vβ15 are expanded by stimulation with TSST-1,[10] and mouse Vβ15 contains a tyrosine at position 56.[31]

On the other hand, the putative electrostatic interactions or increased buried hydrobicity involved in the hVβ2.1–C10 interaction appear to be at least in part a consequence of engineering the CDR2 and FR3 regions to enhance these effects. Interestingly, the wild-type hVβ2.1 is highly charged at these positions and while the electrostatic effects may be masked to some degree by nearby neutralizing residues (e.g. Glu51 and Glu61), it is possible that there are electrostatic contributions that facilitate the docking of the wild-type hVβ2.1 in an orientation similar to that predicted for hVβ2.1–C10. Sequence analysis of human Vβ regions shows that the combination of lysine residues at positions 53 and 62 are unique to hVβ2.1.[29] While two Vβ regions (Vβ19, Vβ30) have a lysine at position 62, they lack a positive charge within the CDR2. Furthermore, many Vβ regions actually contain aspartic acid or glutamic acid residues at position 53 or 62, which could be detrimental to productive electrostatic interactions with TSST-1, based on our model. While structural studies will be required to examine these issues, the hypothetical model suggests a different three-dimensional orientation of TSST-1 on hVβ2.1 compared to the hVβ2.1–SpeC complex (Figure 9(c)). In this model, TSST-1 does not extend to the CDR3 of hVβ2.1, and it is shifted further toward the FR3 region. While the hVβ2.1 footprints of the TSST-1 and SpeC contact regions may differ, the model predicts that TSST-1 and SpeC have overlapping binding regions on hVβ2.1 in the area of CDR2.

Finally, it is worth noting that the engineering of soluble, high-affinity Vβ receptors for TSST-1 that have half-lives of many hours provides the basis for effective neutralizing agents against TSST-1.[32] Our previous study showed that soluble Vβ domains could be engineered with ~1500-fold higher binding affinity (K_D ~ 5 nM) for the SAg Staphylococcal enterotoxin C3 (SEC3).[15] Soluble forms of these Vβ mutants were effective inhibitors of the *in vitro* activity of SEC3. It is desirable to generate Vβ domains with even higher affinities, since the enterotoxins are toxic at very low concentrations.[4] Thus, this new generation of hVβ2.1 mutants, with greater than 10,000-fold improvements in affinity above the wild-type interaction (K_D value of hVβ2.1–D10 of 180 pM affinity, for example), could be useful as protein-based neutralizing agents against TSST-1.

Materials and Methods

Cloning and yeast display of human Vβ2.1

The gene for human Vβ2.1, residues 1–117, containing the mutation C13A, was cloned into the yeast display vector, pCT302, as a NheI-BamHI fragment.[14,33] This construct contains two epitope tags, HA on the N terminus, and two tandem c-myc tags on the C terminus that serve as internal controls for protein expression. To generate a library of random mutants, the hVβ2.1 gene was amplified from the pCT302 plasmid using flanking primers with a method of error-prone PCR to give a 0.5% error rate (data not shown). The PCR product was transformed along with NheI-BglII digested pCT302 into the yeast strain EBY100, which allows the PCR product to be inserted into the plasmid by homologous recombination.[34,35] The resulting library of approximately 10^6 transformants was grown on selective media for 48 h.

Fluorescence activated cell sorting (FACS)

The randomly mutated hVβ2.1 library was cultured for 36 h at 20 °C in medium containing galactose to induce protein expression. One hundred million cells were incubated with 10 μg/ml of mouse anti-human Vβ2 monoclonal antibody (Beckman Coulter). Cells were stained with a 1:50 dilution of goat F(ab′)2 anti-mouse Ig-RPE (Southern Biotech) and selected on a MoFlo high-speed cell sorter (Cytomation). The most fluorescent cells (1%) were collected, cultured overnight in selective media, and then induced in galactose-containing media for 20 h. For the second sort, about 50×10^6 cells were incubated with a 1:50 dilution of anti c-myc (9E10) antibody (Roche), followed by a 1:50 PE-labeled secondary antibody. For the third sort, cells were incubated with a 1:20 dilution of the anti-human Vβ2 antibody (selecting the top 0.5%), and for the fourth sort cells were incubated with a 1:50 dilution of anti-human Vβ2 antibody (selecting the top 0.25%). After four rounds of sorting, individual clones were obtained by plating on selective media.

Flow cytometry of isolated mutants

Individual yeast clones were cultured in glucose-containing media at 30 °C and induced in galactose-containing media at 20 °C for 30 h. Expression levels of hVβ2.1 were examined by incubating 0.4×10^6 yeast cells with anti-HA antibody (Covance) (1:75 dilution),

anti-c-myc 9E10 antibody (1:75 dilution), or anti-human Vβ2 antibody (1:50 dilution) in PBS-BSA for one hour on ice. After washing, cells were incubated with PE-conjugated secondary antibody (1:50 dilution). TSST-1 binding was measured by incubating cells with various concentrations of biotinylated TSST-1 (Toxin Technology), followed by streptavidin-PE (BD Pharmingen) at a 1:500 dilution. Fluorescence levels were measured using a Coulter Epics XL flow cytometer gating on a healthy yeast population.

Affinity maturation of hVβ2.1

The genes encoding stabilized hVβ2.1 mutants were amplified using site-directed mutagenesis with overlapping degenerate primers (with NNS codons). Five residues in the CDR2 (50, 51, 52, 52a and 53) were randomized by this method. DNA from stabilized mutant clones EP-6, 7, 8, 9, 11, and 12 were pooled in equal amounts to use as the template DNA for the PCR. PCR products were incorporated into the yeast display plasmid pCT302 by homologous recombination to generate a library of 14×10^6 independent transformants. The CDR2 library was sorted using a similar approach as described above, except that yeast cells were incubated with decreasing concentrations of biotinylated TSST-1 for each round of sorting, followed by a 1:1000 dilution of streptavidin-PE. Yeast cells were sorted through four cycles, and clones isolated from the fourth cycle were plated on selective media for further analysis.

In a second round of affinity maturation, clones R9, R17, and R18 were used as templates. Libraries were constructed in CDR1 (residues 27, 27a, 28, 29 and 30), CDR2 (residues 52a, 53, 54, 55 and 56), and HV4 (residues 68, 69, 70, 71, and 72). To select for higher affinity mutants with increased off-rates, the three libraries were pooled in equal amounts, incubated with 5 nM biotinylated-TSST-1 for 1 h on ice, followed by an incubation with a tenfold molar excess of unlabeled TSST-1 for 2 h at 25 °C. Yeast cells were selected using these conditions through four cycles of sorting, and clones from the third and fourth cycle were plated.

Alanine scanning mutagenesis

Alanine residues were introduced into the human Vβ2.1 clone C10 in the following residues: CDR1 (Q28, T30), CDR2 (R50, I51, D52, F52a, H53, T55, Y56), FR3/HV4 (V61, K62, D63, K64, L66, N68, H69), and CDR3 (S98, S101). In addition two surface-exposed residues not predicted to be near the binding interface, K40 and E85, were included as controls. These single-site alanine mutations were constructed using the PCR method of splicing by overlap extension. The single-site mutants were transformed into yeast along with linearized pCT302 plasmid. Mutations were confirmed by sequencing and expression of the alanine mutants on the surface of the yeast was induced as described above. Alanine mutants were analyzed individually by flow cytometry.

Surface plasmon resonance

Affinity-matured variants of hVβ2.1 were expressed in *E. coli* and refolded *in vitro* from inclusion bodies as described for murine Vβ8.2 variants affinity-matured for SEC3 binding.[30] Affinity and kinetic analyses of the interactions between hVβ2.1 variants and TSST-1 were determined using a BIAcore 3000 SPR instrument (BIAcore) in 10 mM Hepes buffer containing 150 mM sodium chloride, 3.4 mM EDTA and 0.005% (v/v) surfactant P-20, at 25 °C. TSST-1 at a concentration of 20 μg/ml in 10 mM sodium acetate (pH 4.6) was immobilized (~250 resonance units) to a CM5 sensor chip (Biacore) using standard amine coupling methods. Staphylococcal entertoxin B (SEB) in an equivalent surface density was used as the control surface, as there is no specific binding between hVβ2.1 and SEB. All of the binding experiments were carried out at a flow rate of 25 μl/min. Pulses of 10 mM HCl were used to regenerate both surfaces between injections. SPR data for association (k_a) and dissociation (k_d) rates, as well as the dissociation constant (K_D) were determined by globally fitting the data from different concentrations to a simple 1:1 Langmuir binding model using BIAevaluation software version 4.1. For the EP-8 variant, which exhibits kinetics that are not possible to measure accurately by SPR, the affinity (K_D) was determined by the Scatchard analysis of equilibrium binding of varying concentrations.

A competition assay to determine if TSST-1 and SpeC compete for binding of hVβ2.1 was performed using a CM5 sensorchip with SpeC (~500 RU) immobilized *via* standard amine coupling. Serial dilutions of the stabilized hVβ2.1 mutant EP-8 (100 μM–0.39 μM) were injected over the SpeC surface. Non-linear regression analysis yielded an affinity of ~6 μM for the EP-8–SpeC interaction (data not shown). For the competition experiment, mixtures of EP-8 and TSST-1 were injected over the SpeC surface. The concentration of EP-8 was held constant at 12.5 μM while the concentration of TSST-1 was varied from 100 μM to 12.5 μM. As a control, an identical experiment was performed, in which SEB, which does not bind to EP-8/hVβ2.1, was used.

Molecular modeling

A model of C10 hVβ2.1 was constructed using the coordinates of hVβ2.1 in complex with SpeC (PDB accession code 1KTK). The C10 model was subjected to energy minimizations using the Gromos96 reaction field in Swiss PDB DeepView. Minimizations were performed using 50 steps of steepest descent and 50 steps of conjugate gradient. The model of the hVβ2.1–TSST-1 complex was based on the C10 energy minimized model and the crystal structure of TSST-1 (PDB accession code 2TSS). The molecules were docked manually using the program MacPyMOL† and all structural representations were prepared using MacPyMOL.

Acknowledgements

We thank the staff of the University of Illinois Biotechnology Center for assistance in flow sorting and for DNA sequencing, and Patrick Schlievert, Roy Mariuzza, and Sina Bavari for helpful discussions. This work was supported by National Institutes of Health grants GM55767 and AI064611 (to D.M.K.) and AI55882 (to E.J.S.). R.A.B. was partially supported by an NIH training grant (T32 GM07283). B.M. is a recipient of the Boston Biomedical Research Institute Scholar Award.

† www.pymol.org.

References

1. Todd, J., Fishaut, M., Kapral, F. & Welch, T. (1978). Toxic-shock syndrome associated with phage-group-I Staphylococci. *Lancet*, **2**, 1116–1118.
2. Schlievert, P. M., Shands, K. N., Dan, B. B., Schmid, G. P. & Nishimura, R. D. (1981). Identification and characterization of an exotoxin from *Staphylococcus aureus* associated with toxic-shock syndrome. *J. Infect. Dis.* **143**, 509–516.
3. Bergdoll, M. S., Crass, B. A., Reiser, R. F., Robbins, R. N. & Davis, J. P. (1981). A new staphylococcal enterotoxin, enterotoxin F, associated with toxic-shock-syndrome *Staphylococcus aureus* isolates. *Lancet*, **1**, 1017–1021.
4. McCormick, J. K., Yarwood, J. M. & Schlievert, P. M. (2001). Toxic shock syndrome and bacterial superantigens: an update. *Annu. Rev. Microbiol.* **55**, 77–104.
5. Kappler, J., Kotzin, B., Herron, L., Gelfand, E. W., Bigler, R. D., Boylston, A. *et al*. (1989). V beta-specific stimulation of human T cells by staphylococcal toxins. *Science*, **244**, 811–813.
6. Marrack, P. & Kappler, J. (1990). The staphylococcal entertoxins and their relatives. *Science*, **248**, 705–711.
7. Prasad, G. S., Earhart, C. A., Murray, D. L., Novick, R. P., Schlievert, P. M. & Ohlendorf, D. H. (1993). Structure of toxic shock syndrome toxin 1. *Biochemistry*, **32**, 13761–13766.
8. Acharya, K. R., Passalacqua, E. F., Jones, E. Y., Harlos, K., Stuart, D. I., Brehm, R. D. & Tranter, H. S. (1994). Structural basis of superantigen action inferred from crystal structure of toxic-shock syndrome toxin-1. *Nature*, **367**, 94–97.
9. Sundberg, E. J., Li, Y. & Mariuzza, R. A. (2002). So many ways of getting in the way: diversity in the molecular architecture of superantigen-dependent T-cell signaling complexes. *Curr. Opin. Immunol.* **14**, 36–44.
10. Choi, Y., Kotzin, B., Herron, L., Callahan, J., Marrack, P. & Kappler, J. (1989). Interaction of *Staphylococcus aureus* toxin "superantigens" with human T cells. *Proc. Natl Acad. Acad. Sci. USA*, **86**, 8941–8945.
11. Choi, Y., Lafferty, J. A., Clements, J. R., Todd, J. K., Gelfand, E. W., Kappler, J. *et al*. (1990). Selective expansion of T cells expressing V beta 2 in toxic shock syndrome. *J. Exp. Med*, **172**, 981–984.
12. Sundberg, E. J., Li, H., Llera, A. S., McCormick, J. K., Tormo, J., Schlievert, P. M. *et al*. (2002). Structures of two streptococcal superantigens bound to TCR beta chains reveal diversity in the architecture of T cell signaling complexes. *Structure (Camb)*, **10**, 687–699.
13. McCormick, J. K., Tripp, T. J., Llera, A. S., Sundberg, E. J., Dinges, M. M., Mariuzza, R. A. & Schlievert, P. M. (2003). Functional analysis of the TCR binding domain of toxic shock syndrome toxin-1 predicts further diversity in MHC class II/superantigen/TCR ternary complexes. *J. Immunol.* **171**, 1385–1392.
14. Boder, E. T. & Wittrup, K. D. (1997). Yeast surface display for screening combinatorial polypeptide libraries. *Nature Biotech.* **15**, 553–557.
15. Kieke, M. C., Sundberg, E., Shusta, E. V., Mariuzza, R. A., Wittrup, K. D. & Kranz, D. M. (2001). High affinity T cell receptors from yeast display libraries block T cell activation by superantigens. *J. Mol. Biol.* **307**, 1305–1315.
16. Kieke, M. C., Shusta, E. V., Boder, E. T., Teyton, L., Wittrup, K. D. & Kranz, D. M. (1999). Selection of functional T cell receptor mutants from a yeast surface- display library. *Proc. Natl Acad. Sci. USA*, **96**, 5651–5656.
17. Shusta, E. V., Holler, P. D., Kieke, M. C., Kranz, D. M. & Wittrup, K. D. (2000). Directed evolution of a stable scaffold for T-cell receptor engineering. *Nature Biotechnol.* **18**, 754–759.
18. Shusta, E. V., Kieke, M. C., Parke, E., Kranz, D. M. & Wittrup, K. D. (1999). Yeast polypeptide fusion surface display levels predict thermal stability and soluble secretion efficiency. *J. Mol. Biol.* **292**, 949–956.
19. Bentley, G. A., Boulot, G., Karjalainen, K. & Mariuzza, R. A. (1995). Crystal structure of the β chain of a T cell antigen receptor. *Science*, **267**, 1984–1987.
20. Garcia, K. C., Degano, M., Stanfield, R. L., Brunmark, A., Jackson, M. R., Peterson, P. A. *et al*. (1996). An αβ T cell receptor structure at 2.5 angstrom and its orientation in the TCR-MHC complex. *Science*, **274**, 209–219.
21. Malchiodi, E. L., Eisenstein, E., Fields, B. A., Ohlendorf, D. H., Schlievert, P. M., Karjalainen, K. & Mariuzza, R. A. (1995). Superantigen binding to a T cell receptor β chain of known three-dimensional structure. *J. Exp. Med.* **182**, 1833–1845.
22. Fields, B. A., Malchiodi, E. L., Li, H., Ysern, X., Stauffacher, C. V., Schlievert, P. M. *et al*. (1996). Crystal structure of a T-cell receptor β-chain complexed with a superantigen. *Nature*, **384**, 188–192.
23. Li, H., Llera, A., Tsuchiya, D., Leder, L., Ysern, X., Schlievert, P. M. *et al*. (1998). Three-dimensional structure of the complex between a T cell receptor beta chain and the superantigen staphylococcal enterotoxin B. *Immunity*, **9**, 807–816.
24. Li, H., Llera, A., Malchiodi, E. L. & Mariuzza, R. A. (1999). The structural basis of T cell activation by superantigens. *Annu. Rev. Immunol.* **17**, 435–466.
25. Boder, E. T. & Wittrup, K. D. (1998). Optimal screening of surface-displayed polypeptide libraries. *Biotechnol. Prog.* **14**, 55–62.
26. Boder, E. T., Midelfort, K. S. & Wittrup, K. D. (2000). Directed evolution of antibody fragments with monovalent femtomolar antigen-binding affinity. *Proc. Natl Acad. Sci. USA*, **97**, 10701–10705.
27. Chlewicki, L. K., Holler, P. D., Monti, B. C., Clutter, M. A. & Kranz, D. M. (2005). High-affinity, peptide-specific T cell receptors can be generated by mutations in CDR1, CDR2 or CDR3. *J. Mol. Biol.* **346**, 223–239.
28. Chao, G., Cochran, J. R. & Wittrup, K. D. (2004). Fine epitope mapping of anti-epidermal growth factor receptor antibodies through random mutagenesis and yeast surface display. *J. Mol. Biol.* **342**, 539–550.
29. Arden, B., Clark, S. P., Kabelitz, D. & Mak, T. W. (1995). Human T-cell receptor variable gene segment families. *Immunogenetics*, **42**, 455–500.
30. Yang, J., Swaminathan, C. P., Huang, Y., Guan, R., Cho, S., Kieke, M. C. *et al*. (2003). Dissecting cooperative and additive binding energetics in the affinity maturation pathway of a protein-protein interface. *J. Biol. Chem.* **278**, 50412–50421.
31. Arden, B., Clark, S., Kabelitz, D. & Mak, T. W. (1995). Mouse T-cell receptor variable gene segment families. *Immunogenetics*, **42**, 501–530.
32. Burnett, J. C., Henchal, E. A., Schmaljohn, A. L. & Bavari, S. (2005). The evolving field of biodefence: therapeutic developments and diagnostics. *Nature Rev. Drug Discov.* **4**, 281–297.
33. Holler, P. D., Holman, P. O., Shusta, E. V., O'Herrin, S., Wittrup, K. D. & Kranz, D. M. (2000). In vitro

evolution of a T cell receptor with high affinity for peptide/MHC. *Proc. Natl Acad. Sci. USA*, **97**, 5387–5392.
34. Raymond, C. K., Pownder, T. A. & Sexson, S. L. (1999). General method for plasmid construction using homologous recombination. *Biotechniques*, **26**, 134–138.
35. Starwalt, S. E., Masteller, E. L., Bluestone, J. A. & Kranz, D. M. (2003). Directed evolution of a single-chain class II MHC product by yeast display. *Protein Eng.* **16**, 147–156.

Edited by I. Wilson

(Received 29 June 2005; received in revised form 16 August 2005; accepted 18 August 2005)
Available online 6 September 2005